Development (2014) 141, 2260-2270 doi:10.1242/dev.103705

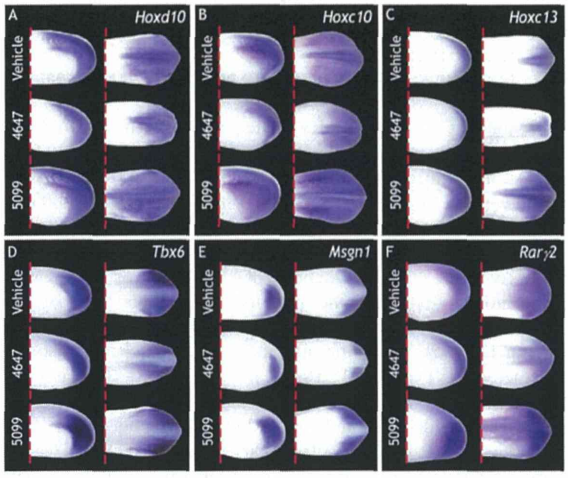

Fig. 2. Posterior Hox and PSM markers are reduced by RARγ-selective agonist and expanded by RARγ-selective inverse agonist. (A-F) WISH from embryos treated post-gastrulation (stage 12.5) with 10 nM 4647, 0.5 μM 5099 or vehicle (0.1% ethanol). Dashed red line represents half the embryo axis. 4647 diminishes and 5099 expands the expression of (A) *Hoxd10* (4647, 16/16; 5099, 17/17 embryos), (B) *Hoxc10* (4647, 14/14; 5099, 21/21), (C) *Hoxc13* (4647, 12/12; 5099, 16/16), (D) *Tbx6* (4647, 11/12; 5099, 17/17), (E) *Msgn1* (4647, 15/15; 5099, 14/14), and (F) *Rarγ2* (4647, 15/15; 5099, 9/9) relative to control vehicle. Embryos shown in lateral or dorsal view at tailbud stage, anterior to left.

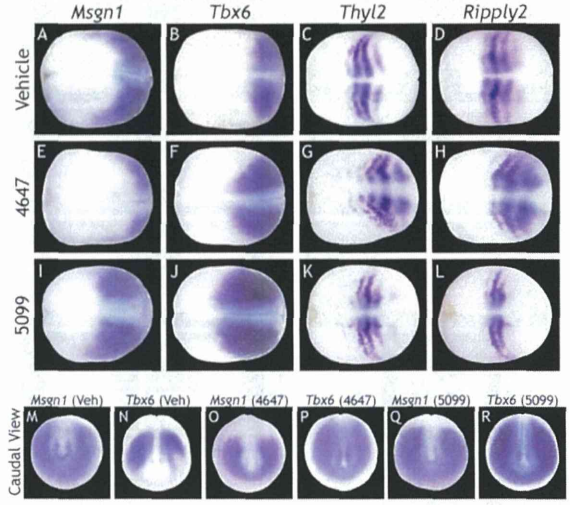

Fig. 3. PSM markers are modulated by RARγ-selective agonist and inverse agonist. (A-R) WISH from embryos treated post-gastrulation (stage 12.5) with 10 nM 4647, 0.5 μM 5099 or vehicle (0.1% ethanol). (A-D) Control expression of *Msgn1*, *Tbx6*, *Thyl2* and *Ripply2*. (E) *Msgn1* expression diminished by 4647 treatment (17/17 embryos). (F) *Tbx6* expression expanded by 4647 treatment (22/22). (G,H) Somitomere domains of *Thyl2* (19/19) and *Ripply2* (17/17) are thicker and posteriorly expanded. (I,J) *Msgn1* (17/17) and *Tbx6* (13/13) expression expanded by 5099 treatment. (K,L) Somitomere domains of *Thyl2* (15/17) and *Ripply2* (26/26) are fewer and thinner. Embryos are shown in dorsal view at neurula stage, anterior to left. (M-R) Caudal views of *Msgn1* and *Tbx6*.

doses of 4647 create embryos lacking anterior and posterior structures, as indicated by the absence of mid/hindbrain markers *En2* and *Krox20* and of posterior gene *Hoxc10* (supplementary material Fig. S9C-F).

Msgn1 and *Tbx6* were upregulated by inverse agonist and downregulated by agonist in the microarray analysis (Table 1). *Msgn1* and *Tbx6* domains were reduced at tailbud stages by post-gastrulation treatment of embryos with 4647, whereas expression was expanded in embryos treated with inverse agonist 5099 (Fig. 2D,E). However, in neurula stage embryos, 4647 reduced *Msgn1* expression while *Tbx6* expression was expanded (Fig. 3E,F,O,P). Expression of *Tbx6* and *Msgn1* was expanded by 5099 (Fig. 3I,J,Q,R), an effect that was more pronounced at higher doses (supplementary material Fig. S10I,J,Q,R). Somitomere markers *Thyl2* and *Ripply2* showed thicker domains; S–III expanded to the posteriormost edge of the embryo where somites are not found in controls (Fig. 3G,H). At non-receptor-selective doses, 4647 exacerbated the phenotypes of *Msgn1*, *Tbx6* and *Ripply2* (supplementary material Fig. S10E,F,H,O,P) and promoted ectopic expression of *Thyl2* in the midline, with somitomeres occupying nearly the entire anteroposterior axis (supplementary material Fig. S10G). By contrast, 5099 treatment produced fewer, thinner somitomeres (Fig. 3K,L), an effect more pronounced at higher doses (supplementary material Fig. S10K,L).

Since *Rarγ2* is co-expressed with *Msgn1*, we expected that 4647 would reduce and 5099 would expand *Rarγ2* expression. *Rarγ2* expression was expanded by inverse agonist and reduced by agonist (Fig. 2F) as verified by QPCR (supplementary material Fig. S11), which is surprising given that other receptor subtypes (RARα2 and RARβ2) are induced by agonist (Leroy et al., 1991; Sucov et al., 1990). The data indicate that 5099 enhances repression by RARγ, increasing caudal gene expression, whereas 4647 relieves repression by RARγ, diminishing caudal gene expression.

Relief of repression reduces domains of posterior Hox and PSM markers

Treatment with 4647 activates RARγ and removes repressors from RARγ targets, creating posterior truncations. We hypothesized that loss of RARγ2 would phenocopy 4647 treatment once RARγ2-mediated repression was lost. We designed AUG MOs to capture both pseudoalleles of *Rarγ2*. Knockdown of RARγ2.1/2.2 resulted in loss of *Hoxc10*, *Hoxd10*, *Hoxa11* and *Hoxc13* expression, together with severe curvature and reduction of the injected side (Fig. 4A-D). Microinjection of splice-blocking MO capturing both pseudoalleles of *Rarγ2* reduced the expression of *Rarγ2* as measured by QPCR, phenocopying the AUG MOs (supplementary material Fig. S12). We demonstrated that axial truncation on the injected side was not due to developmental delay (supplementary material Fig. S13). To establish that RARγ2 is solely responsible for the axial truncations and reduction in posterior Hox and PSM domains, we showed that *Rarγ2* MO can only be rescued with *Rarγ2*, but not *Rarα2* or *Rarβ2*, mRNA (Fig. 5). RARγ2 knockdown reduced and shifted the expression of *Msgn1* and *Tbx6* anteriorly along the midline (Fig. 4E,F,I-J′) and caused an anterior shift in the paraxial domains of *Thyl2* and *Ripply2*, while obliterating lateral expression (Fig. 4G,H). The complexity of the *Rarγ2* MO phenotype is likely to be due to the fact that RARγ2 knockdown both disrupts its repressive function in the absence of ligand and its activation in the presence of ligand, particularly near the determination wavefront.

When the dominant-negative co-repressor c-SMRT is overexpressed, it binds RAR and blocks recruitment of co-repressors (Chen et al., 1996). We identified several c-SMRT isoforms from *Xenopus*, selecting that most similar to human c-SMRT that we used previously. Microinjection of *Xenopus laevis* (Xl) *c-smrt* mRNA relieved

Development (2014) 141, 2260-2270 doi:10.1242/dev.103705

repression by GAL4-xRARγ in whole embryos (supplementary material Fig. S14). This effect was potentiated by addition of 1 μM TTNPB (supplementary material Fig. S14). Overexpression of Xl *c-smrt* mRNA caused significant reductions in the neural and lateral domains of *Hoxc10* and *Hoxd10* (Fig. 6B,D). Xl *c-smrt* also reduced *Hoxc13*, *Tbx6*, *Msgn1* and *xNot* (Fig. 6F,H,H′,J,J′,L). Similar to *Rarγ2* MO, moderate truncation of injected axes was observed in 70% of embryos, but the midline, rostral shifting of *Tbx6* and *Msgn1* (as in *Rarγ2* MO embryos) was minimal. We conclude that Xl c-SMRT relieves repression of *Rarγ2*, causing loss of progenitor and PSM cells and posterior Hox gene expression.

Another method for relieving repression is overexpression of constitutively active VP16-RARγ2 (RARγ2 fused to the VP16 activation domain). Microinjection of VP16-*Rarγ2* mRNA led to a truncated axis on the injected side in 100% of embryos and loss of *Hoxc10*, *Hoxd10*, *Msgn1* and *Tbx6* expression (Fig. 7). These embryos were less curved than *Rarγ2* MO-injected or *c-smrt*-injected embryos, but rostral expansion of neural/midline and lateral domains was consistently observed, similar to *Rarγ2* MO embryos.

Increased repression expands posterior Hox and PSM markers

Treatment with 4647 or microinjection of *c-smrt* or VP16-*Rarγ2* mRNA relieved repression by RARγ, increasing RAR signaling, decreasing posterior Hox and PSM markers. Decreasing RAR signaling should produce the opposite effect. We microinjected mRNA overexpressing the RA catabolic enzyme CYP26A1 and observed rostral shifts in the lateral and neural expression domains of *Hoxc10* and *Hoxd10* (supplementary material Fig. S15). Microinjection of dominant-negative (DN)-RARγ2 should phenocopy 5099 treatment because co-repressors would be retained on RARγ2 targets, leading to repression. Overexpression of DN-RARγ2 increased the expression of *Msgn1* and *Tbx6* in both lateral and paraxial domains, and shifted *xNot* expression rostrally

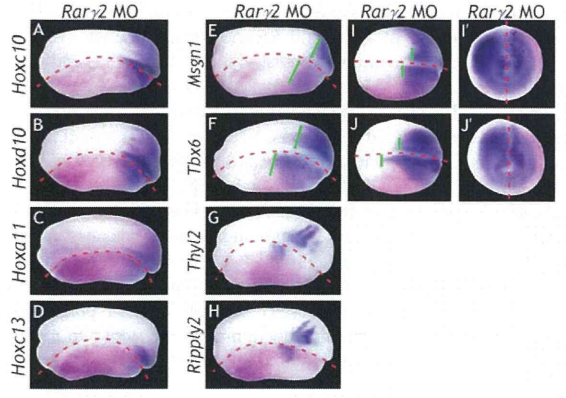

Fig. 4. RARγ2 knockdown alters expression of posterior Hox and PSM markers. (A-J′) Embryos were injected unilaterally at the 2- or 4-cell stage with 7.5 ng *Rarγ2.1* MO+7.5 ng *Rarγ2.2* MO. Injected side is indicated by magenta β-gal lineage tracer. *Rarγ2.1/2.2* MO decreases expression of (A) *Hoxc10* (18/18 embryos), (B) *Hoxd10* (12/12), (C) *Hoxa11* (9/9) and (D) *Hoxc13* (16/16) in tailbud stage embryos. *Rarγ2.1/2.2* MO decreases lateral, but expands midline, expression (green lines) of (E) *Msgn1* (10/13) and (F) *Tbx6* (8/11), knocking down and shifting expression rostrally of (G) *Thyl2* (13/15) and (H) *Ripply2* (13/14) in tailbud stage embryos. *Rarγ2.1/2.2* MO decreases lateral, but expands midline, expression (green lines) of (I) *Msgn1* (35/36) and (J) *Tbx6* (20/20) in neurula stage embryos. Embryos shown in dorsal view with anterior on left. (I′,J′) Caudal views of I and J.

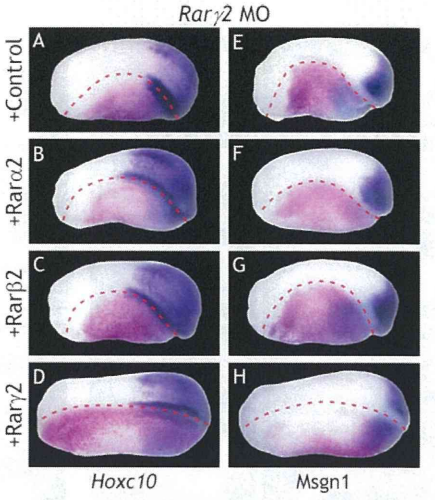

Fig. 5. *Rarγ2* mRNA rescues posterior Hox and PSM expression in *Rarγ2* MO embryos. (A-H) Embryos injected unilaterally at 2- or 4-cell stage. Injected side is indicated by magenta β-gal lineage tracer. (A,E) 5 ng *Rarγ2.1* MO+5 ng *Rarγ2.2* MO+control (*mCherry*) mRNA diminishes *Hoxc10* and *Msgn1* expression, curving the embryo axis in 100% of embryos (*Hoxc10*, 23/23; *Msgn1*, 13/13). (B,C,F,G) Co-injection of *Rarγ2* MO and 1 ng *Rarα2* mRNA or 1 ng *Rarβ2* does not rescue the phenotype; however, (D,H) 1 ng *Rarγ2* mRNA partially rescues axial curvature and *Hoxc10* (18/23) and *Msgn1* (23/35) expression. Tailbud embryos shown in dorsal view with anterior to left.

(Fig. 8B,D,F). DN-RARγ2 phenocopied the effects of *Cyp26a1* mRNA (Moreno and Kintner, 2004) on somitomere markers *Thyl2* and *Ripply2;* rostral shifting and knockdown of somitomere expression was the phenotype that we observed (Fig. 8H,J,K).

Microinjection of *Rarγ2* MO alone resulted in knockdown of *Hoxc10* and axial truncation (Fig. 9A,B,E). We hypothesized that this phenotype was due to loss of repression, reasoning that the phenotype should be rescued with DN-RARγ2. Axial defects and lateral knockdown of *Hoxc10* expression were partially recovered with DN-*Rarγ2* mRNA (Fig. 9C,D,E). The neural domain of *Hoxc10* expression was rescued in nearly all embryos and a rostral shift often observed. We conclude that increasing repression with DN-RARγ2 or overexpressing CYP26A1 (removing ligand) promotes caudal gene expression, similar to chemical treatment with 5099. Moreover, loss of caudal structures and gene expression due to *Rarγ2* MO are rescued by restoring repression with DN-RARγ2.

DISCUSSION

RARγ repression in caudal development

Most studies consider only one aspect of RAR signaling, namely its role as a ligand-activated transcription factor promoting the expression of target genes. In developmental biology, RA signaling has been studied extensively for its ability to promote differentiation and establish boundaries in somitogenesis, neurogenesis and rhombomere segmentation (reviewed by Rhinn and Dolle, 2012). Liganded RAR has been predicted to function passively in the caudal region until required to facilitate body axis cessation (Olivera-Martinez et al., 2012), when somitogenesis is nearing completion because the determination wavefront, moving the RA source caudally, has exhausted the progenitor cell pool (Gomez and Pourquie, 2009). Here, liganded RARγ would function as an activator promoting apoptosis (Shum et al., 1999) at terminal tailbud stage. However, this does not address why RARγ2 would be highly expressed where RA is

Development (2014) 141, 2260-2270 doi:10.1242/dev.103705

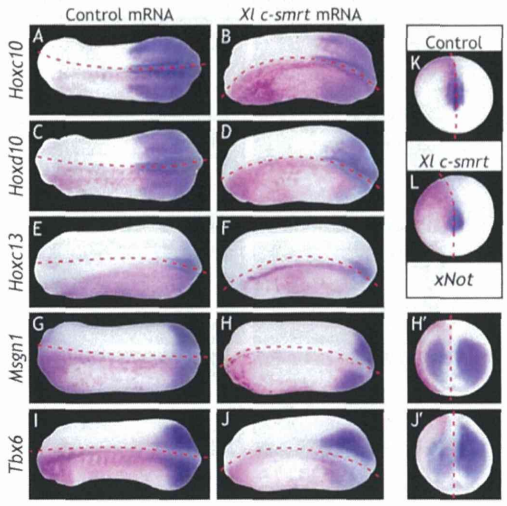

Fig. 6. c-SMRT overexpression knocks down posterior Hox, PSM and CNH markers. Embryos injected unilaterally at 2- or 4-cell stage with 4 ng *c-smrt* mRNA or control (*mCherry*) mRNA. Injected side indicated by magenta β-gal lineage tracer. (A,C,E,G,I,K) Control expression of *Hoxc10*, *Hoxd10*, *Hoxc13*, *Msgn1*, *Tbx6* and *xNot*. (B,D,F,H,J,L) *c-smrt* overexpression shortens the axis on injected side in 70% of embryos. (B) *c-smrt* mRNA results in lateral knockdown (13/23 embryos), neural knockdown (7/23) or neural rostral shift (7/23) in *Hoxc10* expression. (D) *c-smrt* mRNA produces neural and lateral knockdown (15/19) or lateral knockdown alone (4/19) of *Hoxd10* expression. (F,H,J) *c-smrt* mRNA knocks down expression of *Hoxc13* (14/18), *Msgn1* (12/14) and *Tbx6* (15/15). Tailbud embryos shown with anterior to left. (H',J') Caudal views of H and J. (L) *c-smrt* mRNA knocks down *xNot* (12/15) expression in neurula stage embryos (caudal view, dorsal to top).

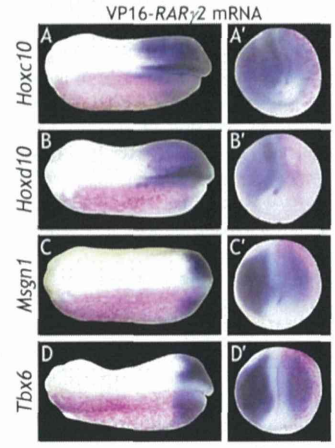

Fig. 7. VP16-RARγ2 overexpression knocks down posterior Hox and PSM marker expression. Embryos injected unilaterally at 2- or 4-cell stage with 0.3 ng VP16-*Rarγ2* mRNA or control (*mCherry*) mRNA. Injected side is indicated by magenta β-gal lineage tracer. Control expression of *Hoxc10*, *Hoxd10*, *Msgn1* and *Tbx6* is shown in Fig. 6A,C,G,I. (A-D) VP16-*Rarγ2* overexpression shortens the axis on injected side in 100% of embryos. (A,B) VP16-*Rarγ2* mRNA results in neural/midline rostral shift and lateral knockdown in *Hoxc10* (9/13 embryos) and *Hoxd10* (7/13) expression. Neural/midline knockdown is also observed (*Hoxc10*, 4/13; *Hoxd10*, 7/13). (C,D) VP16-*Rarγ2* mRNA rostrally shifts and/or knocks down *Msgn1* (12/12) and *Tbx6* (13/13) expression. Tailbud embryos shown with anterior to left. (A'-D') Caudal views of A-D.

presumed absent due to CYP26A1 expression. Here we show that RARγ is engaged in all stages of caudal development, not solely as a terminator of the body axis. RARγ functions as an unliganded repressor required for the maintenance of the posterior PSM and progenitor cell population that allows axial elongation (Fig. 10). RARγ acts as a liganded activator in the anterior, segmented PSM to facilitate somite differentiation (Fig. 10). Repression mediated by the unliganded receptor–co-repressor complex constitutes a novel mechanism by which posterior markers are upregulated during axial elongation in *Xenopus* embryos.

Our microarray results suggest that axial elongation is regulated by RAR-mediated repression. Enhancing repression with AGN193109 upregulated, and activation of RAR by TTNPB downregulated, many posterior Hox, PSM and CNH genes in neurula stage embryos. We identified AGN193109-upregulated genes expressed in PSM (Table 1) that are mostly absent from regions of somite maturation (Blewitt, 2009; Yoon et al., 2000). The CNH markers *xBra3* and *xNot* were also upregulated by AGN193109, thus both PSM and CNH markers were upregulated by enhancing RAR repression and downregulated by increasing RAR activation. Current literature suggests the existence of a negative-feedback loop between these two populations of cells: *Msgn1* is induced by *Brachyury* and *Wnt8* in CNH but represses their expression to promote PSM fates (Fior et al., 2012; Yabe and Takada, 2012). Our results support a novel role of RAR repression in the maintenance of cells in both unsegmented PSM and stem-like CNH.

We showed that *X. laevis* RARα, RARβ and RARγ can repress basal transcriptional activity in the absence of RA and examined whether this repression is physiologically relevant in caudal development. *Rarγ2* is expressed in embryonic regions where it might actively repress genes involved in axial elongation. *Rarγ2* is synexpressed with the PSM marker *Msgn1* and overlaps with *Tbx6*, *Hoxc10*, the S–III domains of *Thyl2* and *Ripply2*, and the CNH marker *xNot*. By contrast, *Rarγ2* is expressed at low levels in trunk (where *Myod* and *Rarα* are expressed) and in the anterior, segmented PSM expression domains of *Thyl2* and *Ripply2*. Since absence of RA is required for the proliferation and/or survival of caudal PSM and CNH cells, the presence of RARγ in posterior tissue would be contradictory if it functioned as an activator. We infer that RARγ acts as a repressor throughout unsegmented PSM and CNH where RA is absent, but as an activator of somitomere markers near the differentiation wavefront where *Rarγ2* overlaps with S–III and where *Raldh2* expression indicates the presence of RA. It remains unknown what repressors RARγ targets to indirectly upregulate caudal genes. One possibility is that RARγ represses *Ripply2*, which functions to repress *Tbx6* (reviewed by Dahmann et al., 2011), as supported by the observation that increasing activation with 4647 expands *Ripply2* posteriorly. Hence, RARγ would normally function in the posterior to repress *Ripply2*, therefore promoting expression of *Tbx6*.

RARγ repression promotes the maintenance of unsegmented PSM and CNH

Since high doses of 4647 result in embryos consisting largely of trunk, it is predictable that nearly the entire embryo differentiated into somitomeres (with thicker boundaries). At lower, RARγ-selective 4647 doses, somitomeres were shifted posteriorly and thickened. This phenotype, which is also seen with RA treatment or FGF inhibition by SU5402, was attributed to increased numbers of cells allocated to somitomeres and a decreased progenitor pool (Dubrulle et al., 2001; Moreno and Kintner, 2004). 5099 upregulates both *Tbx6* and *Msgn1*, indicating that unsegmented PSM is expanded by increased RAR

Development (2014) 141, 2260-2270 doi:10.1242/dev.103705

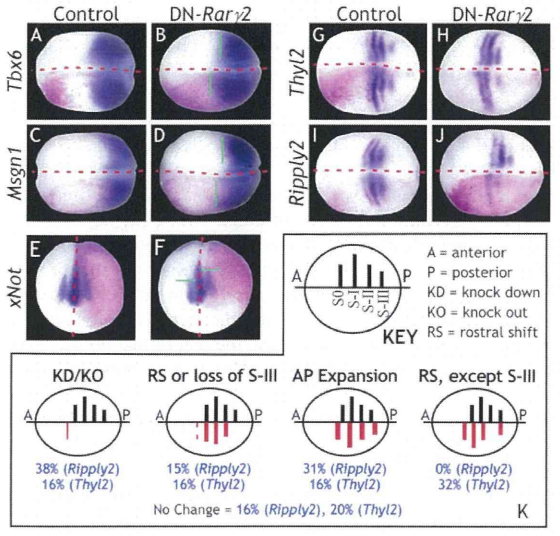

Fig. 8. Overexpression of DN-*Rarγ2* mRNA expands expression of PSM and CNH markers, shifting or knocking down somitomere markers *Thyl2* and *Ripply2*. (A-J) Embryos injected unilaterally at 2- or 4-cell stage. Injected side is indicated by magenta β-gal lineage tracer. (A,C,E,G,I) Control (*mCherry*) mRNA does not alter expression of *Tbx6*, *Msgn1*, *Thyl2*, *Ripply2* or *xNot*. (B,D,F) 2 ng DN-*Rarγ2* mRNA expands expression of *Msgn1* (8/11) and *Tbx6* (15/23) (green lines) and rostrally shifts *xNot* (8/10). (H,J) DN-*Rarγ2* overexpression produces multiple phenotypes of *Thyl2* and *Ripply2* expression, as characterized and scored in K. Neurula embryos shown in dorsal view with anterior to left.

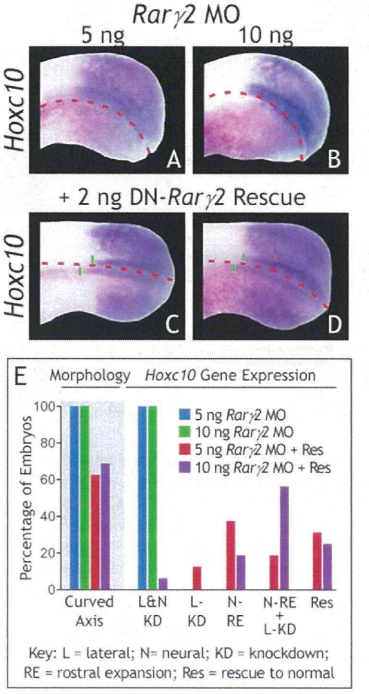

Fig. 9. DN-*Rarγ2* mRNA rescues posterior Hox expression in *Rarγ2* MO embryos. (A-D) Embryos injected unilaterally at 2- or 4-cell stage. Injected side is indicated by magenta β-gal lineage tracer. (A) 2.5 ng *Rarγ2.1* MO +2.5 ng *Rarγ2.2* MO or (B) 5 ng *Rarγ2.1* MO+5 ng *Rarγ2.2* MO diminishes *Hoxc10* expression and curves the embryo axis. (C,D) 2 ng DN-*Rarγ2* mRNA partially rescues this effect and expands neural expression of *Hoxc10*. Tailbud embryos shown in dorsal view with anterior to left. (E) Detailed scoring of the rescue experiment.

repression. However, we note distinct differences in the effects of 4647 on *Tbx6* versus *Msgn1*. *Tbx6* is upregulated by 4647 at early stages but downregulated at later stages, as also observed for the T-box gene *Tbx1* (Janesick et al., 2012). Unlike *Msgn1*, *Tbx6* plays a dual role in the unsegmented PSM and the determination front where it controls the anteroposterior patterning of somitomeres via *Ripply2* (Hitachi et al., 2008).

Msgn1 expression does not overlap somitomeres and functions to maintain unsegmented PSM by encouraging the differentiation of caudal stem cells. Loss of *Msgn1* expression leads to smaller somitomeres owing to the accumulation of bipotential progenitor cells that have not received signals to commit to PSM fate (Fior et al., 2012; Yabe and Takada, 2012). Treatment with 4647 also leads to loss of *Msgn1* and thus somitomeres should be smaller; however, they are larger. Despite such divergent early stage phenotypes, *Msgn1*$^{-/-}$ embryos (Yoon and Wold, 2000) and 4647 embryos both display fewer somites and reduced caudal structures at late stages. Caudal progenitors cannot be instructed to become somites in *Msgn1*$^{-/-}$ embryos. In 4647-treated embryos, the pool is expeditiously transformed into thickened somitomeres early, but the progenitor supply is exhausted before axial elongation is complete, reducing somitomere numbers. That 4647 can differentiate somitomeres at all without *Msgn1* is intriguing. Either *Tbx6* compensates for *Msgn1* knockdown, or 4647 can induce uncommitted, non-PSM progenitor cells to differentiate into somitomeres.

Relief of RARγ repression suppresses PSM and CNH marker gene expression

If RARγ2 functions solely as a repressor, then RARγ2 knockdown should induce a loss of repression phenotype. *Rarγ2* MO microinjection resulted in severely truncated body axes with caudal PSM and posterior Hox markers significantly reduced at tailbud stages, similar to 4647 treatment. This phenotype was attributed to axial defects, not merely developmental delay. We noted three differences between 4647-treated and *Rarγ2* MO-injected embryos. First, axes of *Rarγ2* MO embryos were significantly curved, which was attributed to imbalance/dominance of the uninjected side versus the truncated injected side. Second, caudal PSM markers, while qualitatively reduced with *Rarγ2* MO, also expanded rostrally, even when accounting for shortened axes on injected sides. Third, thickened, posteriorly expanded somitomeres were not seen with *Rarγ2* MO. RARγ2 acting as an activator near the somitogenesis front where RA is present would explain some discrepancies. RA functions in the determination wavefront to antagonize proliferating PSM and promote somitomere differentiation (Moreno and Kintner, 2004). If RA acts through RARγ2 in the wavefront, then loss of *Rarγ2* should expand unsegmented PSM and reduce somitomere expression, exactly as observed.

Axial curvature and loss of *Hoxc10* and *Msgn1* expression in *Rarγ2* MO-injected embryos could be rescued by *Rarγ2*, but not *Rarα2* or *Rarβ2* mRNA. Therefore, *Rarγ2* is the sole receptor responsible for axial elongation, in agreement with *Rarγ2* as the only RAR expressed in caudal domains. *Rarβ2* is present only in trunk and pharyngeal arches (Escriva et al., 2006) and *Rarα2* is completely absent from the blastopore and surrounding area (see figure S1A,B in the supplementary material of Janesick et al.,

Development (2014) 141, 2260-2270 doi:10.1242/dev.103705

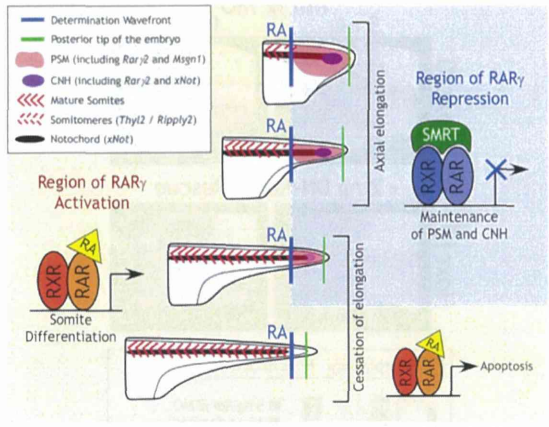

Fig. 10. RARγ functions as both transcriptional activator and repressor during somitogenesis and axial elongation. RARγ is activated by RA near the determination wavefront where PSM differentiates into somitomeres, then mature somites. The progenitor pool within the PSM and CNH domains, which is maintained by *Rarγ* repression, feeds into the wavefront until exhausted, as somitogenesis proceeds faster than progenitors are replenished (Gomez and Pourquie, 2009). As PSM and CNH domains diminish, the distance between RA/wavefront (blue line) and the posterior tip of the embryo (green line) becomes shorter. RA is able to enter the posterior, activating *Rarγ*, switching its function from repressor promoting growth to activator terminating growth. RXR, retinoid X receptor.

2013). *Hoxc10* expression could be rescued in *Rarγ2* MO-injected embryos by co-injecting DN-*Rarγ2* mRNA, definitively establishing that RARγ2 functions as a repressor in the caudal domain. DN-RARγ2 restored *Hoxc10* expression, especially in neural tube, where additional rostral expansion was often observed. DN-RARγ2 rescue restored curved axes only partially. We predict that axial curvature is a loss-of-activation effect inhibiting somitomere formation; therefore, the phenotype should not be rescued by DN-RARγ2, but rescued by wild-type RARγ2, as we observed.

Perhaps the most direct method for relieving repression of RARγ2 in caudal regions is overexpression of dominant-negative co-repressor c-SMRT, which binds RARγ2 preventing recruitment of co-repressors and thereby blocking repression. c-SMRT overexpression resulted in truncated axes with loss of posterior Hox, unsegmented PSM and CNH markers, but not rostral shifting of *Msgn1* and *Tbx6* as had been observed for *Rarγ2* MO embryos. This indicates that rostral shifting in *Rarγ2* MO embryos results from loss of activation rather than relief of repression. We previously showed that c-SMRT not only relieves repression of RAR but also potentiates ligand-mediated activation (Koide et al., 2001). Since c-SMRT was expressed ubiquitously, it could superactivate RARα or RARγ where RA is present. It should also be noted that c-SMRT can interact with other nuclear receptors and transcription factors. Therefore, we can only conclude that c-SMRT overexpression inhibits maintenance of the caudal PSM and progenitor pool (where RA is absent). We cannot draw conclusions about somitomere markers in c-SMRT overexpression embryos since their expression is controlled by RAR activation, which c-SMRT does not reduce.

RAR signaling and posterior Hox gene regulation

We identified a novel function for RARγ as a transcriptional repressor in the regulation of posterior Hox genes. Posterior Hox genes pattern caudal embryonic regions, promote axial elongation (Young et al., 2009) and are linked to cell cycle progression (Gabellini et al., 2003) and therefore proliferation. Axial elongation involves the addition of tissue, as cells must proliferate to contribute segments. Normally, FGF and RA signaling are mutually antagonistic, but we provide evidence that RARγ can support proliferative mechanisms in the absence of RA.

Hox gene expression was altered by 4647 and 5099 treatment, even post-gastrulation. Hence, although Hox gene expression is initiated collinearly during gastrulation, this temporal pattern is not immutable. In support of this model, axial progenitor cells transplanted to anterior locations do not retain their previous Hox identity (McGrew et al., 2008). Furthermore, manipulation of anteroposterior locations of PSM and the determination wavefront resulted in corresponding changes in Hox gene expression (Iimura et al., 2009; Wellik, 2007). We showed that 4647 treatment pushes determination fronts caudally and observed posterior regressions of *Hoxc10*, *Hoxd10* and *Hoxc13* expression. Conversely, rostral expansion in PSM by increasing RAR repression was accompanied by anterior shifts in posterior Hox expression. Owing to posterior prevalence, rostral shifts of *Hoxc10* or *Hoxd10* expression could indicate that thoracic segments will develop caudal structures at later stages. Similarly, rostral shifts in *Hoxc13* could drive lumbar segments to sacral morphology. Homeotic transformations from manipulating RAR repression deserve future study.

Conclusions

We conclude that the RAR-mediated repression of caudal genes is crucial for axial elongation, establishing another important role for active repression by nuclear receptors in body axis extension, as previously shown for head formation (Koide et al., 2001). RARγ2 is likely to function as an activator near the determination wavefront and a repressor to maintain axial progenitor pools in the PSM and CNH. As axial elongation nears completion, RARγ2 functions as an activator because the progenitor pool is exhausted and RA comes into close proximity to the caudal domain of RARγ2, where it can then promote apoptosis and terminate the body axis. This model is attractive because it utilizes the same protein to activate or repress target genes depending on the proximity to RA and explains the high levels of posterior RARγ2 expression. RARγ2 is likely to function in multiple steps of somitogenesis and axial elongation (Fig. 10): (1) preservation of undifferentiated states in the progenitor pools (marked by the CNH); (2) maintenance of PSM; (3) initiation of somitomere differentiation; and (4) axial termination. Future studies require RARγ target gene identification because very few ChIP studies have ascertained direct targets, and even fewer studies have explored subtype-selective RAR targets. In the case of inverse agonist-upregulated genes (the focal point of our study), identifying repressors of PSM and progenitors will be key, as these genes are likely to be targeted by unliganded RAR in a classic 'repression of a repressor' mechanism.

MATERIALS AND METHODS

Percellome microarray analysis

Xenopus laevis eggs from three different females were fertilized *in vitro* and embryos staged as described (Janesick et al., 2012). Stage 7 embryos were treated in groups of 25 in 60-mm Petri dishes with 10 ml 0.1× MBS containing 1 μM RAR agonist (TTNPB), 1 μM RAR inverse agonist (AGN193109) or vehicle control (0.1% ethanol). Three dishes per treatment per female were collected (27 dishes total: three technical replicates, three biological replicates per treatment). Each dish of embryos was harvested at stage 18 into 1.5 ml RNAlater (Invitrogen) and stored at 4°C. Samples were homogenized, RNA isolated and DNA quantitated (Kanno et al., 2006). Graded-dose spiked cocktail

Development (2014) 141, 2260-2270 doi:10.1242/dev.103705

(GSC) made of five *Bacillus subtilis* RNA sequences present on Affymetrix GeneChip arrays (AFFX-ThrX-3_at, AFFX-LysX-3_at, AFFX-PheX-3_at, AFFX-DapX-3_at, AFFX-TrpnX-3_at) was added to the sample homogenates in proportion to their DNA concentration (Kanno et al., 2006). GSC-spiked sample homogenates were processed and probes synthesized using standard Affymetrix protocols, applied to *Xenopus* microarray v1.0 GeneChips and analyzed using Percellome software (Kanno et al., 2006). Absolutized mRNA levels were expressed as copy number per cell for each probe set.

Percellome microarray data were analyzed using CyberT (Kayala and Baldi, 2012). We did not use low value thresholding/offsetting or log/VSN normalizations. Bayesian analysis used a sliding window of 101 and confidence value of 10. The *P*-values reported are Bonferroni corrected and Benjamini and Hochber corrected. The full microarray dataset is available at GEO under accession number GSE57352. Genes included in Table 1 comprise a subset upregulated by AGN193109/downregulated by TTNPB based on their regional expression in the posterior.

Embryo microinjection

Xenopus eggs were fertilized *in vitro* and embryos staged as described (Janesick et al., 2012). Embryos were injected bilaterally or unilaterally at the 2- or 4-cell stage with gene-specific morpholinos (MOs) (supplementary material Table S1) and/or mRNA together with 100 pg/embryo β-galactosidase (β-gal) mRNA. For all MO experiments, control embryos were injected with 10 ng standard control MO (GeneTools). Embryos were maintained in 0.1× MBS until appropriate stages. Embryos processed for WISH were fixed in MEMFA, stained with magenta-GAL (Biosynth), and then stored in 100% ethanol (Janesick et al., 2012).

pCDG1-DN-*xRarγ2* was constructed by cloning amino acids 1-393 (lacking the AF-2 domain) into the *Nco*I-*Bam*HI site of pCDG1 (Blumberg et al., 1998). pCDG1-VP16-*xRarγ2* was constructed by cloning the VP16 activation domain upstream of *xRarγ2* into pCDG1. pCDG1-*xRaraα2*, pCMX-GAL4-*Raraα* and GAL4-*Rarγ* were from Blumberg et al. (Blumberg et al., 1996). *X. laevis Rarβ1* and *Rarβ2* sequences were found by aligning to the *X. tropicalis* sequences. pCDG1-*xRarβ2* and pCMX-GAL4-*xRarβ* cloning primers are listed in supplementary material Table S2. pCDG1-*xCyp26a1* and pCDG1-*c-smrt* were constructed by PCR amplification of *xCyp26a1* coding regions (Hollemann et al., 1998) or Xl *c-smrt* (37b−, 41+) (Chen et al., 1996; Malartre et al., 2004) and cloning into pCDG1.

xRaraα1$^{EGCKG\rightarrow GSCKV}$, *xRaraα2*$^{EGCKG\rightarrow GSCKV}$, *xRarβ2*$^{EGCKG\rightarrow GSCKV}$, *xRarγ1*$^{EGCKG\rightarrow GSCKV}$ and *xRarγ2*$^{EGCKG\rightarrow GSCKV}$ were designed according to Klein et al. (1996), constructed by two-fragment PCR, and cloned into pCDG1 (primer sequences are provided in supplementary material Table S3). Four copies of RXRE$^{1/2}$-GRE$^{1/2}$ (GGAAGGGTTCACCGAA-AGAACACTCGC) were cloned upstream of the TK-luciferase reporter. All pCDG1 plasmids were sequence verified, linearized with *Not*I, and mRNA transcribed using mMessage mMachine T7 (Ambion). pCS2-*mCherry* was linearized with *Not*I and transcribed from the SP6 promoter.

Embryo treatments and reporter assays

Microinjected embryos were treated at stage 8 with the following chemicals (in 0.1× MBS): TTNPB (RAR agonist), NRX204647 (RARγ-selective agonist), NRX205099 (RARγ-selective inverse agonist) or 0.1% ethanol vehicle. Twenty-five embryos were treated in each 60-mm Petri dish containing 10 ml chemical. Treated embryos were fixed in MEMFA and processed for WISH, or separated into five-embryo aliquots at stage 10.5 for luciferase assays, or separated into five-embryo aliquots at neurula or tailbud stage for QPCR as described (Janesick et al., 2012). Each group of five embryos was considered one biological replicate (n=1).

WISH

Embryos were microinjected or treated with chemicals after the completion of gastrulation (stage 12.5). WISH was performed as previously described (Janesick et al., 2012). *Rarγ1*, *Rarγ2*, *Raraα* (Blumberg et al., 1992), *Hoxc10*, *Ripply2*, *Thyl2*, *Msgn1* (Klein et al., 2002), *Hoxd10* (Lombardo and Slack, 2001), *Tbx6* (Uchiyama et al., 2001), *Raldh2* (Glinka et al., 1996) and *Myod* (Hopwood et al., 1989) probes were prepared by PCR amplification of coding regions from cDNA with T7 promoter at the 3′ end and *in vitro* transcribed. *Hoxc13* sequence was derived from EST clone XL042b19. Relevant primers are listed in supplementary material Table S4. *Krox20* (Bradley et al., 1993) and *En2* (Bolce et al., 1992) probes were made using T7 and T3 polymerase from *Eco*RI and *Xba*I linearized plasmids, respectively. Probes were transcribed with MEGAscript T7 (Ambion) in the presence of digoxigenin-11-UTP (Roche). Double WISH was conducted as described (Janesick et al., 2012). DNP-*Rarγ2* was transcribed in the presence of dinitrophenol-11-UTP (PerkinElmer). *Hoxc10* expression was quantitated using MATLAB (MathWorks) (supplementary material Fig. S8). The number of purple pixels was calculated by thresholding individual RGB channels (R&B>170, G>120) and dividing by the total number of pixels occupied by the embryo.

Transfection

1 µg CMX-*Rar*$^{EGCKG\rightarrow GSCKV}$ effector plasmid was co-transfected with 5 µg tk-(RXRE$^{1/2}$-GRE$^{1/2}$)×4 luciferase reporter and 5 µg pCMX-β-galactosidase transfection control plasmids as previously described (Chamorro-Garcia et al., 2012). For activation assays, NRX204647 was tested from 10^{-11} M to 10^{-5} M. For antagonism assays, NRX205099 was tested from 10^{-10} M to 10^{-5} M against 10^{-8} M 9-cis RA. All transfections were performed in triplicate and reproduced in multiple experiments. Data are reported as normalized luciferase±s.e.m. or percentage reduction±s.e.m. using standard propagation of error (Bevington and Robinson, 2003).

Quantitative real-time reverse transcription PCR (QPCR)

Total RNA from five-embryo pools was DNase treated, LiCl precipitated, and reverse transcribed into cDNA (Janesick et al., 2012). First-strand cDNA was quantitated in a Light Cycler 480 System (Roche) using primer sets listed in supplementary material Table S5 and SYBR Green. Each primer set amplified a single band as determined by gel electrophoresis and melting curve analysis. QPCR data for supplementary material Figs S2 and S7 were analyzed by ΔCt relative to *Histone H4*, correcting for amplification efficiency between RARs (Pfaffl, 2001). QPCR data for supplementary material Figs S11 and S12 were analyzed by ΔΔCt relative to *Histone H4*, normalizing to control embryos. Error bars represent biological replicates calculated using standard propagation of error.

Acknowledgements

We thank Connie Chung for technical help during the early stages of this study and Dr Dennis Bittner for editorial assistance.

Competing interests

The authors declare no competing financial interests.

Author contributions

T.T.L.N. performed WISH. K.A., K.I., S.K. and J.K. executed the Percellome microarray experiment. R.A.S.C. provided 4647 and 5099 chemicals with advice on use. A.J. and B.B. designed, supervised and performed experiments, and wrote, edited and submitted the manuscript.

Funding

Supported by grants from the National Science Foundation (NSF) [IOS-0719576, IOS-1147236 to B.B.]. A.J. was a predoctoral trainee of NSF IGERT DGE 0549479. K.I., S.K. and J.K. were funded by Health Sciences Research Grant H15-kagaku-002 from the Ministry of Health, Labour and Welfare, Japan.

Supplementary material

Supplementary material available online at
http://dev.biologists.org/lookup/suppl/doi:10.1242/dev.103705/-/DC1

References

Abu-Abed, S., Dollé, P., Metzger, D., Beckett, B., Chambon, P. and Petkovich, M. (2001). The retinoic acid-metabolizing enzyme, CYP26A1, is essential for normal hindbrain patterning, vertebral identity, and development of posterior structures. *Genes Dev.* **15**, 226-240.

Arima, K., Shiotsugu, J., Niu, R., Khandpur, R., Martinez, M., Shin, Y., Koide, T., Cho, K. W. Y., Kitayama, A., Ueno, N. et al. (2005). Global analysis of RAR-responsive genes in the Xenopus neurula using cDNA microarrays. *Dev. Dyn.* **232**, 414-431.

Beck, C. W. and Slack, J. M. W. (1998). Analysis of the developing Xenopus tail bud reveals separate phases of gene expression during determination and outgrowth. *Mech. Dev.* **72**, 41-52.

Bevington, P. R. and Robinson, D. K. (2003). *Data Reduction and Error Analysis for the Physical Sciences*. New York: McGraw-Hill Education.

Blewitt, R. (2009). Enhancer of split-related-2 mRNA shows cyclic expression during somitogenesis in Xenopus laevis. *Biosci. Horizons* **2**, 22-31.
Blumberg, B., Mangelsdorf, D. J., Dyck, J. A., Bittner, D. A., Evans, R. M. and De Robertis, E. M. (1992). Multiple retinoid-responsive receptors in a single cell: families of retinoid "X" receptors and retinoic acid receptors in the Xenopus egg. *Proc. Natl. Acad. Sci. U.S.A.* **89**, 2321-2325.
Blumberg, B., Bolado, J., Jr, Derguini, F., Craig, A. G., Moreno, T. A., Chakravarti, D., Heyman, R. A., Buck, J. and Evans, R. M. (1996). Novel retinoic acid receptor ligands in Xenopus embryos. *Proc. Natl. Acad. Sci. U.S.A.* **93**, 4873-4878.
Blumberg, B., Bolado, J., Jr, Moreno, T. A., Kintner, C., Evans, R. M. and Papalopulu, N. (1997). An essential role for retinoid signaling in anteroposterior neural patterning. *Development* **124**, 373-379.
Blumberg, B., Kang, H., Bolado, J., Chen, H., Craig, A. G., Moreno, T. A., Umesono, K., Perlmann, T., De Robertis, E. M. and Evans, R. M. (1998). BXR, an embryonic orphan nuclear receptor activated by a novel class of endogenous benzoate metabolites. *Genes Dev.* **12**, 1269-1277.
Bolce, M. E., Hemmati-Brivanlou, A., Kushner, P. D. and Harland, R. M. (1992). Ventral ectoderm of Xenopus forms neural tissue, including hindbrain, in response to activin. *Development* **115**, 681-688.
Bradley, L. C., Snape, A., Bhatt, S. and Wilkinson, D. G. (1993). The structure and expression of the Xenopus Krox-20 gene: conserved and divergent patterns of expression in rhombomeres and neural crest. *Mech. Dev.* **40**, 73-84.
Buchberger, A., Bonneick, S. and Arnold, H.-H. (2000). Expression of the novel basic-helix-loop-helix transcription factor cMespo in presomitic mesoderm of chicken embryos. *Mech. Dev.* **97**, 223-226.
Cambray, N. and Wilson, V. (2002). Axial progenitors with extensive potency are localised to the mouse chordoneural hinge. *Development* **129**, 4855-4866.
Cambray, N. and Wilson, V. (2007). Two distinct sources for a population of maturing axial progenitors. *Development* **134**, 2829-2840.
Chakravarti, D., LaMorte, V. J., Nelson, M. C., Nakajima, T., Schulman, I. G., Juguilon, H., Montminy, M. and Evans, R. M. (1996). Role of CBP/P300 in nuclear receptor signalling. *Nature* **383**, 99-103.
Chamorro-García, R., Kirchner, S., Li, X., Janesick, A., Casey, S. C., Chow, C. and Blumberg, B. (2012). Bisphenol A diglycidyl ether induces adipogenic differentiation of multipotent stromal stem cells through a peroxisome proliferator-activated receptor gamma-independent mechanism. *Environ. Health Perspect.* **120**, 984-989.
Chen, J. D. and Evans, R. M. (1995). A transcriptional co-repressor that interacts with nuclear hormone receptors. *Nature* **377**, 454-457.
Chen, J. D., Umesono, K. and Evans, R. M. (1996). SMRT isoforms mediate repression and anti-repression of nuclear receptor heterodimers. *Proc. Natl. Acad. Sci. U.S.A.* **93**, 7567-7571.
Dahmann, C., Oates, A. C. and Brand, M. (2011). Boundary formation and maintenance in tissue development. *Nat. Rev. Genet.* **12**, 43-55.
Davis, R. L. and Kirschner, M. W. (2000). The fate of cells in the tailbud of Xenopus laevis. *Development* **127**, 255-267.
de Roos, K., Sonneveld, E., Compaan, B., ten Berge, D., Durston, A. J. and van der Saag, P. T. (1999). Expression of retinoic acid 4-hydroxylase (CYP26) during mouse and Xenopus laevis embryogenesis. *Mech. Dev.* **82**, 205-211.
Dequéant, M.-L. and Pourquié, O. (2008). Segmental patterning of the vertebrate embryonic axis. *Nat. Rev. Genet.* **9**, 370-382.
Dubrulle, J., McGrew, M. J. and Pourquié, O. (2001). FGF signaling controls somite boundary position and regulates segmentation clock control of spatiotemporal Hox gene activation. *Cell* **106**, 219-232.
Escriva, H., Bertrand, S., Germain, P., Robinson-Rechavi, M., Umbhauer, M., Cartry, J., Duffraisse, M., Holland, L., Gronemeyer, H. and Laudet, V. (2006). Neofunctionalization in vertebrates: the example of retinoic acid receptors. *PLoS Genet.* **2**, e102.
Fior, R., Maxwell, A. A., Ma, T. P., Vezzaro, A., Moens, C. B., Amacher, S. L., Lewis, J. and Saude, L. (2012). The differentiation and movement of presomitic mesoderm progenitor cells are controlled by Mesogenin 1. *Development* **139**, 4656-4665.
Fujii, H., Sato, T., Kaneko, S., Gotoh, O., Fujii-Kuriyama, Y., Osawa, K., Kato, S. and Hamada, H. (1997). Metabolic inactivation of retinoic acid by a novel P450 differentially expressed in developing mouse embryos. *EMBO J.* **16**, 4163-4173.
Gabellini, D., Colaluca, I. N., Vodermaier, H. C., Biamonti, G., Giacca, M., Falaschi, A., Riva, S. and Peverali, F. A. (2003). Early mitotic degradation of the homeoprotein HOXC10 is potentially linked to cell cycle progression. *EMBO J.* **22**, 3715-3724.
Glinka, A., Delius, H., Blumenstock, C. and Niehrs, C. (1996). Combinatorial signalling by Xwnt-11 and Xnr3 in the organizer epithelium. *Mech. Dev.* **60**, 221-231.
Gomez, C. and Pourquié, O. (2009). Developmental control of segment numbers in vertebrates. *J. Exp. Zool. B Mol. Dev. Evol.* **312B**, 533-544.
Hitachi, K., Kondow, A., Danno, H., Inui, M., Uchiyama, H. and Asashima, M. (2008). Tbx6, Thylacine1, and E47 synergistically activate bowline expression in Xenopus somitogenesis. *Dev. Biol.* **313**, 816-828.
Hollemann, T., Chen, Y., Grunz, H. and Pieler, T. (1998). Regionalized metabolic activity establishes boundaries of retinoic acid signalling. *EMBO J.* **17**, 7361-7372.
Hopwood, N. D., Pluck, A. and Gurdon, J. B. (1989). MyoD expression in the forming somites is an early response to mesoderm induction in Xenopus embryos. *EMBO J.* **8**, 3409-3417.
Iimura, T., Denans, N. and Pourquié, O. (2009). Establishment of Hox vertebral identities in the embryonic spine precursors. *Curr. Top. Dev. Biol.* **88**, 201-234.
Janesick, A., Shiotsugu, J., Taketani, M. and Blumberg, B. (2012). RIPPLY3 is a retinoic acid-inducible repressor required for setting the borders of the pre-placodal ectoderm. *Development* **139**, 1213-1224.
Janesick, A., Abbey, R., Chung, C., Liu, S., Taketani, M. and Blumberg, B. (2013). ERF and ETV3L are retinoic acid-inducible repressors required for primary neurogenesis. *Development* **140**, 3095-3106.
Kanno, J., Aisaki, K.-i., Igarashi, K., Nakatsu, N., Ono, A., Kodama, Y. and Nagao, T. (2006). "Per cell" normalization method for mRNA measurement by quantitative PCR and microarrays. *BMC Genomics* **7**, 64.
Kayala, M. A. and Baldi, P. (2012). Cyber-T web server: differential analysis of high-throughput data. *Nucleic Acids Res.* **40**, W553-W559.
Klein, E. S., Pino, M. E., Johnson, A. T., Davies, P. J. A., Nagpal, S., Thacher, S. M., Krasinski, G. and Chandraratna, R. A. S. (1996). Identification and functional separation of retinoic acid receptor neutral antagonists and inverse agonists. *J. Biol. Chem.* **271**, 22692-22696.
Klein, S. L., Strausberg, R. L., Wagner, L., Pontius, J., Clifton, S. W. and Richardson, P. (2002). Genetic and genomic tools for Xenopus research: the NIH Xenopus initiative. *Dev. Dyn.* **225**, 384-391.
Koide, T., Downes, M., Chandraratna, R. A. S., Blumberg, B. and Umesono, K. (2001). Active repression of RAR signaling is required for head formation. *Genes Dev.* **15**, 2111-2121.
Lamka, M. L., Boulet, A. M. and Sakonju, S. (1992). Ectopic expression of UBX and ABD-B proteins during Drosophila embryogenesis: competition, not a functional hierarchy, explains phenotypic suppression. *Development* **116**, 841-854.
Leroy, P., Nakshatri, H. and Chambon, P. (1991). Mouse retinoic acid receptor alpha 2 isoform is transcribed from a promoter that contains a retinoic acid response element. *Proc. Natl. Acad. Sci. U.S.A.* **88**, 10138-10142.
Lombardo, A. and Slack, J. M. (2001). Abdominal B-type Hox gene expression in Xenopus laevis. *Mech. Dev.* **106**, 191-195.
Malartre, M., Short, S. and Sharpe, C. (2004). Alternative splicing generates multiple SMRT transcripts encoding conserved repressor domains linked to variable transcription factor interaction domains. *Nucleic Acids Res.* **32**, 4676-4686.
McGrew, M. J., Sherman, A., Lillico, S. G., Ellard, F. M., Radcliffe, P. A., Gilhooley, H. J., Mitrophanous, K. A., Cambray, N., Wilson, V. and Sang, H. (2008). Localised axial progenitor cell populations in the avian tail bud are not committed to a posterior Hox identity. *Development* **135**, 2289-2299.
Mollard, R., Viville, S., Ward, S. J., Décimo, D., Chambon, P. and Dollé, P. (2000). Tissue-specific expression of retinoic acid receptor isoform transcripts in the mouse embryo. *Mech. Dev.* **94**, 223-232.
Moreno, T. A. and Kintner, C. (2004). Regulation of segmental patterning by retinoic acid signaling during Xenopus somitogenesis. *Dev. Cell* **6**, 205-218.
Nakaya, Y., Kuroda, S., Katagiri, Y. T., Kaibuchi, K. and Takahashi, Y. (2004). Mesenchymal-epithelial transition during somitic segmentation is regulated by differential roles of Cdc42 and Rac1. *Dev. Cell* **7**, 425-438.
Nowotschin, S., Ferrer-Vaquer, A., Concepcion, D., Papaioannou, V. E. and Hadjantonakis, A.-K. (2012). Interaction of Wnt3a, Msgn1 and Tbx6 in neural versus paraxial mesoderm lineage commitment and paraxial mesoderm differentiation in the mouse embryo. *Dev. Biol.* **367**, 1-14.
Olivera-Martinez, I., Harada, H., Halley, P. A. and Storey, K. G. (2012). Loss of FGF-dependent mesoderm identity and rise of endogenous retinoid signalling determine cessation of body axis elongation. *PLoS Biol.* **10**, e1001415.
Pfaffl, M. W. (2001). A new mathematical model for relative quantification in real-time RT-PCR. *Nucleic Acids Res.* **29**, e45.
Pfeffer, P. L. and De Robertis, E. M. (1994). Regional specificity of RAR gamma isoforms in Xenopus development. *Mech. Dev.* **45**, 147-153.
Pourquié, O. and Tam, P. P. L. (2001). A nomenclature for prospective somites and phases of cyclic gene expression in the presomitic mesoderm. *Dev. Cell* **1**, 619-620.
Rhinn, M. and Dollé, P. (2012). Retinoic acid signalling during development. *Development* **139**, 843-858.
Sakai, Y., Meno, C., Fujii, H., Nishino, J., Shiratori, H., Saijoh, Y., Rossant, J. and Hamada, H. (2001). The retinoic acid-inactivating enzyme CYP26 is essential for establishing an uneven distribution of retinoic acid along the anterio-posterior axis within the mouse embryo. *Genes Dev.* **15**, 213-225.
Shimono, K., Tung, W.-e., Macolino, C., Chi, A. H.-T., Didizian, J. H., Mundy, C., Chandraratna, R. A., Mishina, Y., Enomoto-Iwamoto, M., Pacifici, M. et al. (2011). Potent inhibition of heterotopic ossification by nuclear retinoic acid receptor-gamma agonists. *Nat. Med.* **17**, 454-460.

Development (2014) 141, 2260-2270 doi:10.1242/dev.103705

Shum, A. S. W., Poon, L. L. M., Tang, W. W. T., Koide, T., Chan, B. W. H., Leung, Y.-C. G., Shiroishi, T. and Copp, A. J. (1999). Retinoic acid induces down-regulation of Wnt-3a, apoptosis and diversion of tail bud cells to a neural fate in the mouse embryo. *Mech. Dev.* **84**, 17-30.

Sive, H. L., Draper, B. W., Harland, R. M. and Weintraub, H. (1990). Identification of a retinoic acid-sensitive period during primary axis formation in Xenopus laevis. *Genes Dev.* **4**, 932-942.

Sucov, H. M., Murakami, K. K. and Evans, R. M. (1990). Characterization of an autoregulated response element in the mouse retinoic acid receptor type beta gene. *Proc. Natl. Acad. Sci. U.S.A.* **87**, 5392-5396.

Takemoto, T., Uchikawa, M., Yoshida, M., Bell, D. M., Lovell-Badge, R., Papaioannou, V. E. and Kondoh, H. (2011). Tbx6-dependent Sox2 regulation determines neural or mesodermal fate in axial stem cells. *Nature* **470**, 394-398.

Tam, P. P. L., Goldman, D., Camus, A. and Schoenwolf, G. C. (2000). 1 Early events of somitogenesis in higher vertebrates: allocation of precursor cells during gastrulation and the organization of a meristic pattern in the paraxial mesoderm. *Curr. Top. Dev. Biol.* **47**, 1-32.

Thacher, S. M., Vasudevan, J. and Chandraratna, R. A. S. (2000). Therapeutic applications for ligands of retinoid receptors. *Curr. Pharm. Des.* **6**, 25-58.

Tsang, K. Y., Sinha, S., Liu, X., Bhat, S. and Chandraratna, R., A. (2003). Disubstituted Chalcone Oximes Having Rar(Gamma)-Retinoid Receptor Antagonist Activity. European Patent Office.

Uchiyama, H., Kobayashi, T., Yamashita, A., Ohno, S. and Yabe, S. (2001). Cloning and characterization of the T-box gene Tbx6 in Xenopus laevis. *Dev. Growth Differ.* **43**, 657-669.

von Dassow, G., Schmidt, J. E. and Kimelman, D. (1993). Induction of the Xenopus organizer: expression and regulation of Xnot, a novel FGF and activin-regulated homeo box gene. *Genes Dev.* **7**, 355-366.

Wellik, D. M. (2007). Hox patterning of the vertebrate axial skeleton. *Dev. Dyn.* **236**, 2454-2463.

Weston, A. D., Blumberg, B. and Underhill, T. M. (2003). Active repression by unliganded retinoid receptors in development: less is sometimes more. *J. Cell Biol.* **161**, 223-228.

Wong, C. W. and Privalsky, M. L. (1998). Transcriptional silencing is defined by isoform- and heterodimer-specific interactions between nuclear hormone receptors and corepressors. *Mol. Cell. Biol.* **18**, 5724-5733.

Yabe, T. and Takada, S. (2012). Mesogenin causes embryonic mesoderm progenitors to differentiate during development of zebrafish tail somites. *Dev. Biol.* **370**, 213-222.

Yoon, J. K. and Wold, B. (2000). The bHLH regulator pMesogenin1 is required for maturation and segmentation of paraxial mesoderm. *Genes Dev.* **14**, 3204-3214.

Yoon, J. K., Moon, R. T. and Wold, B. (2000). The bHLH class protein pMesogenin1 can specify paraxial mesoderm phenotypes. *Dev. Biol.* **222**, 376-391.

Young, T., Rowland, J. E., van de Ven, C., Bialecka, M., Novoa, A., Carapuco, M., van Nes, J., de Graaff, W., Duluc, I., Freund, J.-N. et al. (2009). Cdx and Hox genes differentially regulate posterior axial growth in mammalian embryos. *Dev. Cell* **17**, 516-526.

Genomics Data 2 (2014) 296–298

Contents lists available at ScienceDirect

Genomics Data

journal homepage: http://www.journals.elsevier.com/genomics-data/

Data in Brief

Gene expression response to EWS–FLI1 in mouse embryonic cartilage

Miwa Tanaka [a], Ken-ichi Aisaki [b], Satoshi Kitajima [b], Katsuhide Igarashi [b], Jun Kanno [b], Takuro Nakamura [a,*]

[a] Division of Carcinogenesis, The Cancer Institute, Japanese Foundation for Cancer Research, Tokyo, Japan
[b] Division of Cellular and Molecular Toxicology, Biosafety Research Center, National Institute of Health Science, Tokyo, Japan

ARTICLE INFO

Article history:
Received 21 August 2014
Received in revised form 3 September 2014
Accepted 7 September 2014
Available online 16 September 2014

Keywords:
cDNA microarrays
Embryonic cartilage
EWS–FLI1
Ewing's sarcoma
Gene expression profiling

ABSTRACT

Ewing's sarcoma is a rare bone tumor that affects children and adolescents. We have recently succeeded to induce Ewing's sarcoma-like small round cell tumor in mice by expression of EWS–ETS fusion genes in murine embryonic osteochondrogenic progenitors. The Ewing's sarcoma precursors are enriched in embryonic superficial zone (eSZ) cells of long bone. To get insights into the mechanisms of Ewing's sarcoma development, gene expression profiles between EWS–FLI1-sensitive eSZ cells and EWS–FLI1-resistant embryonic growth plate (eGP) cells were compared using DNA microarrays. Gene expression of eSZ and eGP cells (total, 30 samples) was evaluated with or without *EWS–FLI1* expression 0, 8 or 48 h after gene transduction. Our data provide useful information for gene expression responses to fusion oncogenes in human sarcoma.

Specifications	
Organism/cell line/tissue	*Mus musculus*
Strain	BALB/c, dpc 18.5
Sex	Both male and female
Array type	Affymetrix MOE430 2.0 array
Data format	Raw data: CEL files, processed data: Excel table
Experimental factors	Tissue
Experimental features	Gene expression in eSZ cells and eGP cells with or without EWS–FLI1 expression was compared
Consent	n/a

Direct link to deposited data

Deposited data can be found here: http://www.ncbi.nlm.nih.gov/geo/query/acc.cgi?acc=GSE32618.

Experimental design, materials and methods

Preparation of mouse embryonic superficial zone (eSZ) and growth plate (eGP) cells

Femoral and humeral bones of BALB/c mouse embryos were removed aseptically on 18.5 dpc, and they were microdissected into eSZ and growth plate (eGP) under a stereomicroscope (Zeiss Stemi 2000-C, Carl Zeiss MicroImaging). Each region was minced and gently digested with 2 mg/mL of collagenase (Wako Pure Chemical) at 37 °C for 2 h. They were cultured in growth medium composed of Iscove's Modified Dulbecco's Medium (Invitrogen) supplemented with 15% fetal bovine serum, and subjected immediately to retroviral infection.

Retroviral infection

N-terminal FLAG-tagged *EWS–FLI1* was introduced into the pMYs-IRES-GFP vector. The full length *EWS–FLI1* cDNA was a kind gift from Dr. Susanne Baker. Retroviral infections of eSZ, eGP or shaft cells were performed as described [1]. Infection efficiency was examined using a FACSCalibur flow cytometer (Beckton Dickinson). Cells were harvested after fourty-eight hours of infection.

RNA isolation and microarray

GeneChip analysis was conducted to determine gene expression profiles. The per cell normalization method (Percellome method) was applied to eSZ and eGP samples [2]. Briefly, cellular lysates were prepared with RLT buffer (QIAGEN). A 10 μL aliquot of each lysate was treated with DNAse-free RNase A (Nippon Gene Inc., Japan) for 30 min at 37 °C, followed by Proteinase K (Roche Diagnostics GmbH., Germany) for 3 h at 55 °C. The aliquot was then transferred to a 96-well black plate. PicoGreen fluorescent dye (Molecular Probes Inc., USA) was added to each well, shaken for 10 s four times and then incubated for 2 min at 30 °C. DNA concentration was measured using a 96

* Corresponding author. Tel.: + 81 335700462.
E-mail address: takuro-ind@umin.net (T. Nakamura).

http://dx.doi.org/10.1016/j.gdata.2014.09.003

well fluorescence plate reader with excitation at 485 nm and emission at 538 nm. λ phage DNA (PicoGreen Kit, Molecular Probes Inc., USA) was used as standard. As reported previously [2], the grade-dosed spike cocktails (GSCs) made of the *Bacillus subtilis* RNAs corresponding to the sequences in the Affymetrix GeneChip arrays (AFFX-ThrX-3_at, AFFX-LysX-3_at, AFFX-PheX-3_at, AFFX-DapX-3_at, and AFFX-TrpnX-3_at) were prepared, and GSCs were added to the sample homogenates in proportion to their DNA concentrations. Total RNA was extracted using the RNeasy Mini Kit (QIAGEN). The GeneChip Mouse Genome 430 2.0 Array (Affymetrix) was hybridized with the cRNA generated from eSZ and eGP cells, and murine Ewing's sarcoma tissue (Table 1). After staining with streptavidin–phycoerythrin conjugates, arrays were scanned using an Affymetrix GeneChip Scanner 3000 and analyzed using Affymetrix GeneChip Command Console Software (AGCC, Affymetrix) and GeneSpring GX 11.0.2 (Agilent Technologies) as described previously [3]. The expression data for eSZ and eGP cells were converted to Percellome data, i.e., absolute copy numbers of mRNA per one cell, by the homemade software SCal4 (Spike Calculation version 4). This software also graphically indicates the efficiency of in vitro transcription, the dose–response linearity of the five GSC spikes and the location of spike probe sets in the histogram of all probe sets (Fig. 1A). From the same treatment group (n = 3), all the pairs were plotted to a scatter graph as red (expression above detection level) or green dots (below detection level) with the data of five yellow spike probe sets (Fig. 1B). If any samples did not draw a symmetric scatter plot with yellow dot on the diagonal line, the sample were rejected for evaluation, and they were subjected to additional analyses.

Data analysis

Homemade software named RSort (Roughness Sort) [4] was used. This program sorts the probe sets as upward or downward peaks in a 3D isobologram (Fig. 2). To avoid biologically nonsense probe sets

Table 1
Summary of processed samples.

GEO accession no.	Cell types	Gene transfer	Time (h)
GSM808581	eSZ	No	0
GSM808582	eSZ	No	0
GSM808583	eSZ	No	0
GSM808584	eGP	No	0
GSM808585	eGP	No	0
GSM808586	eGP	No	0
GSM808587	eSZ	Empty vector	8
GSM808588	eSZ	Empty vector	8
GSM808589	eSZ	Empty vector	8
GSM808590	eGP	Empty vector	8
GSM808591	eGP	Empty vector	8
GSM808592	eGP	Empty vector	8
GSM808593	eSZ	EWS–FLI1	8
GSM808594	eSZ	EWS–FLI1	8
GSM808595	eSZ	EWS–FLI1	8
GSM808596	eGP	EWS–FLI1	8
GSM808597	eGP	EWS–FLI1	8
GSM808598	eGP	EWS–FLI1	8
GSM808599	eSZ	Empty vector	48
GSM808600	eSZ	Empty vector	48
GSM808601	eSZ	Empty vector	48
GSM808602	eGP	Empty vector	48
GSM808603	eGP	Empty vector	48
GSM808604	eGP	Empty vector	48
GSM808605	eSZ	EWS–FLI1	48
GSM808606	eSZ	EWS–FLI1	48
GSM808607	eSZ	EWS–FLI1	48
GSM808608	eGP	EWS–FLI1	48
GSM808609	eGP	EWS–FLI1	48
GSM808610	eGP	EWS–FLI1	48

eSZ, embryonic superficial zone; GP, growth plate.

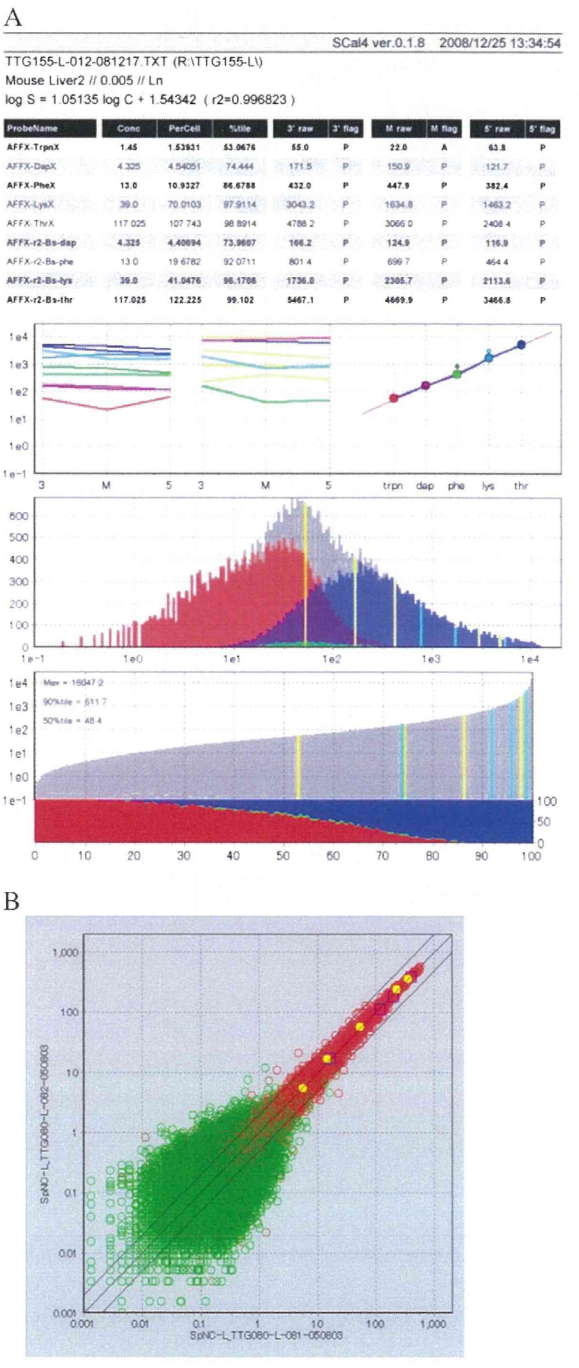

Fig. 1. Evaluation of the microarray data according to the PerCellome method. (A) An example of the SCal4 software report. SCal4 graphically indicates the efficiency of in vitro transcription, the dose–response linearity of the five GSC spikes and the location of spike probe sets in the histogram of all probe sets. (B) A scatter plot of gene expression between two experimental groups. All the pairs of probe sets were plotted to a scatter graph as red (expression above detection level) or green dots (below detection level) with the data of five yellow spike probe sets.